UNSTEADY TURBULENT PROPERTIES IN NEGATIVE WAVES IN OPEN CHANNELS

by Martina Reichstetter ([1]) and Hubert Chanson ([1])

([1]) The University of Queensland, School of Civil Engineering, Brisbane QLD 4072, Australia.

Corresponding author:

Hubert Chanson, Professor

School of Civil Engineering, The University of Queensland

Brisbane QLD 4072, Australia

Fax: (61 7) 33 65 45 99   Email: h.chanson@uq.edu.au

Abstract:

In an open channel, a sudden drop in free-surface elevation is associated with the development of a negative wave. While some simple analytical solution is widely described in textbooks, little research was conducted to date on the unsteady turbulence properties beneath negative waves. A series of new physical experiments were conducted in a rectangular channel. The unsteady free-surface profile and turbulence characteristics were measured in a negative wave propagating upstream against an initially steady flow using non-intrusive acoustic displacement meters, video imagery and acoustic Doppler velocimetry (ADV). For one set of flow conditions, the experiments were repeated 25 times at two longitudinal locations and four vertical elevations to yield ensemble-averaged data. The wave leading edge propagated upstream with a speed which was a function of with time and space. The velocity data showed that the upstream propagation of the negative wave was linked with a gentle drop in water elevation associated with an acceleration of the flow, while some increased turbulence occurred beneath the wave associated with large velocity fluctuations and large Reynolds stress components. The velocity fluctuations and turbulent stresses were significantly larger than in the initially steady flow and in the final flow motion.

Keywords: Negative waves, Open channel flows, Turbulent velocity measurements, Acoustic Doppler velocimetry, Ensemble-average, Unsteady turbulence.

1. INTRODUCTION

In an open channel, a sudden increase in water depth is called a positive surge or bore which is a major flow discontinuity characterised by a steep front with intense mixing beneath. On the other hand, a sudden decrease in water depth, called a negative wave or surge, is characterised by a gentle change in free-surface elevation (Fig. 1). It may occur upstream of an opening gate, as well as downstream of a closing gate (Henderson 1966, Liggett 1994). The generation of a negative surge is of particular relevance to the hydropower industry, when a sudden increase in water demand may induce a drawdown in the hydropower (forebay) canal. The maximum available discharge Q_{max} is set by the open channel hydraulic conditions (Montes 1998, Chanson 2004). For a rectangular channel of width B, it yields:

$$Q_{max} = \frac{8}{27} \sqrt{g} \, d_o{}^{3/2} B \tag{1}$$

where d_o is the initial flow depth in the forebay canal.

A simple solution of the negative wave is commonly treated in fluid mechanics and hydraulics textbooks (Henderson 1966, Lighthill 1978, Liggett 1994). Although a classical data set was the seminal study of Favre (1935), little research was conducted to date on the unsteady turbulence properties beneath negative waves despite the practical relevance, for example to canal and reservoir desilting during drawdown. The present study investigates physically the unsteady flow properties of negative waves under controlled flow conditions. It is the aim of this work to characterise the unsteady open channel flow motion including free-surface properties and velocity field in negative wave and surges

2. PHYSICAL MODELLING AND EXPERIMENTAL PROCEDURES

2.1 Presentation

The physical studies of negative surges and waves are performed with geometrically similar models, and the modelling requires the selection of the relevant similitude. For the simple case of a negative surge propagating in a rectangular, horizontal channel after a sudden and complete gate opening, a dimensional analysis yields:

$$d, V_x, V_y, V_z = F_1\left(x, y, z, t, d_o, V_o, \delta, B, g, \rho, \mu, \sigma...\right) \tag{2}$$

where d is the flow depth, V_x, V_y, V_z are respectively the longitudinal, transverse and vertical velocity components at a location (x, y, z), x is the coordinate in the flow direction, y is the horizontal transverse coordinate measured from the channel centreline, z is the vertical coordinate measured from channel bed, t is the time, d_o and V_o are the initial flow depth and velocity respectively, δ is the initial boundary layer thickness at x, B is the channel width, g is the gravity acceleration, ρ and μ are the water density and dynamic viscosity respectively, and σ is the surface tension between air

and water. Equation (2) expresses the unsteady flow properties (left handside terms) at a point in space (x, y, z) and time t as functions of the initial flow conditions, channel geometry and fluid properties.

Some basic considerations show that the relevant characteristic length and velocity scales are respectively the initial flow depth d_o and velocity V_o. Equation (2) may be rewritten in dimensionless terms:

$$\frac{d}{d_o}, \frac{V_x}{V_o}, \frac{V_y}{V_o}, \frac{V_z}{V_o} = F_2\left(\frac{x}{d_o}, \frac{y}{d_o}, \frac{z}{d_o}, t\sqrt{\frac{g}{d_o}}, \frac{V_o}{\sqrt{gd_o}}, \rho\frac{V_o\,d_o}{\mu}, \frac{\delta}{d_o}, \frac{B}{d_o}, \frac{g\,\mu^4}{\rho\,\sigma^3}, \cdots \right) \qquad (3)$$

In Equation (3) right handside, the fifth and sixth terms are the Froude and Reynolds numbers respectively, and the ninth term is the Morton number.

In a geometrically similar model, a true dynamic similarity is achieved only if each dimensionless parameter has the same value in both model and prototype. Scale effects may exist when one or more Π-terms have different values between the model and prototype. In free-surface flows including negative waves, the gravity effects are important and a Froude similitude is commonly used (Henderson 1966, Chanson 1999). This is also the case in the present study.

2.2 Experimental facility

The experiments were performed in a 12 m long, 0.5 m wide horizontal flume made of smooth PVC bed and glass sidewalls. The water was supplied by a constant head tank feeding a large intake chamber with a smooth convergent into the 12 m long glass-walled channel. A fast-opening gate was located at the channel downstream end x = 11.15 m where x is the longitudinal distance from the channel upstream end (Fig. 1). The tainter gate was identical to that used by Koch and Chanson (2009). The water discharge was measured with two orifice meters which were calibrated on site using a volume per time technique. The percentage of error was less than 2%. In steady flows, the water depths were measured using rail mounted pointer gauges. The unsteady water depth was measured using a series of acoustic displacement meters Microsonic[TM] Mic+25/ IU/TC. The data accuracy and response of the acoustic displacement meters were 0.18 mm and 50 ms respectively. The displacement meters were located at x = 5.6, 6.0, 6.2, 10.2, 10.5, 10.8 m. Additional observations were performed using a digital video camera Panasonic[TM] NV-GS300 (25 fps) and a dSLR camera Pentax[TM] K-7.

Further informations on the experimental facility and instrumentation as well as the full data set reported in Reichstetter and Chanson (2011).

2.3 Acoustic Doppler velocimetry and data post processing

The turbulent velocity components were measured using an acoustic Doppler velocimeter (ADV) Nortek[TM] Vectrino+ (Serial No. VNO 0436) equipped with a side-looking head. The velocity rate was set to 1.0 m/s and the sampling rate was 200 Hz for all the experiments with a data accuracy of 0.01 m/s. The translation of the ADV probe in the vertical direction was controlled by a fine adjustment travelling mechanism connected to a Mitutoyo[TM] digimatic scale unit with an error less than 0.1 mm. Herein all the measurements were taken on the channel centreline, and the ADV and displacement sensors were synchronised and sampled simultaneously at 200 Hz.

In a turbulent flow, the instantaneous velocity V is typically decomposed into an average component $\overline{V}$ and a turbulent fluctuation v: $V = \overline{V} + v$. In an unsteady flow, the long-term trend and the short-term turbulent fluctuations must be processed separately (Bradshaw 1971). A technique consists in the repetition of the same experiment for N times, and $\overline{V}$ is the ensemble-average. In the present study, a series of twenty five instantaneous velocity records were repeated at four vertical elevations (z/d_o = 0.03, 0.11, 0.56 and 0.61) in a manner such that the initial flow conditions were perfectly identical for each run, where z is the vertical elevation and d_o the initial flow depth. An ensemble-median of each instantaneous velocity component was produced for each vertical elevation.

The ADV unit was mounted at x = 6 or 10.5 m. For the two upper locations (z/d_o = 0.56 and 0.61), the sampling was stopped when the ADV head became out of water.

2.4 Experimental flow conditions and negative wave generation

A series of experiments were performed with an initially steady flow rate Q = 0.020 & 0.030 m^3/s and a range of undershoot gate height before fast-opening h = 0.030 to 0.050 m (Table 1, Series 1). The turbulent velocity measurements were conducted for Q = 0.020 m^3/s and h = 0.030 m with an initial water depth d_o = 0.24 m at x = 6 m (Table 1, Series 2).

For each experimental run, the steady gradually-varied flow conditions were established prior to the first measurements. The negative surge was produced by opening rapidly the tainter gate: the opening time was less than 0.15 to 0.2 s. Such an opening time was small enough to have a negligible effect on the surge propagation as shown by Lauber (1997).

Prior to gate opening, the free-surface was controlled by the flow conditions around the tainter gate. The initial free-surface profile is shown in Figure 2 for Q = 0.020 m^3/s. After gate opening, the final free-surface shape (recorded 5 minutes after opening) was controlled by the overfall at the channel downstream end where critical flow conditions

took place. The final free-surface profiles are reported in Figure 2, where the data are compared with the numerical integration of the backwater equation.

The backwater equation is a differential form of the energy equation which yields for a steady open channel flow:

$$\frac{\partial d}{\partial x} = \frac{S_o - S_f}{1 - Fr^2} \qquad (3)$$

where S_o is the bed slope (herein $S_o = 0$), S_f is the friction slope ($S_f = f\, V^2/(2\, g\, D_H)$), f is the Darcy-Weisbach friction factor, DH is the hydraulic diameter ($D_H = 4A/P_w$) with A the flow cross-section area and P_w the wetted perimeter, and Fr is the Froude number (Henderson 1966, Montes 1998, Chanson 2004).

3. BASIC OBSERVATIONS

3.1 Presentation

The visual observations as well as the free surface measurements at the gate showed a steep drop of the water surface next to the gate (e.g. $10 < x < 11.15$ m) immediately after the gate opening (Fig. 3 & Appendix I). Figure 3 presents a series of instantaneous free-surface profiles next to the gate ($10.48 < x < 11.2$ m, Fig. 3A) and further upstream ($5.8 < x < 6.3$ m, Fig. 3B) recorded with the video camera. In Figure 3, d_o is the initial flow depth at $x = 6$ m, x' and x" are positive upstream, and the data were recorded at 25 fps. Some supplementary video data are listed in Appendix I. In both Figure 3 and the video data, the initially steady discharge flowed from right to left, and the negative surge propagated from left to right.

The observations highlighted the rapid gate opening and wave formation (Fig. 3A & movie [23_03_2010_1_short.AVI]), although the disturbance vanished very rapidly, within one second. The instantaneous free-surface exhibited a smooth shape further upstream as seen in Figure 3B and in the movie [2010-05-05 13.41.43 ns5.a_very_short. AVI]. During the upstream wave propagation, the free-surface was very flat and smooth, and the visual observations illustrated the gradual lowering of the water surface during the upstream propagation of the negative surge (movie [2010-05-05 13.41.43 ns5.a_very_short. AVI]). Except next to the gate shortly after opening, the upstream propagation of the negative wave was barely perceptible, as illustrated in the movie [2010-05-05 13.41.43 ns5.a_very_short. AVI].

The celerity of the negative wave leading edge was recorded using a combination of photographic, video and acoustic displacement meter data. Figure 4 presents a typical data set, where x' is the upstream distance from gate. The data showed two distinct trends. Immediately after the gate closure, the negative wave formed rapidly and the celerity of its

leading edge increased with time up to $x'/d_o = 4$. This acceleration phase was associated by some strong flow disturbance as seen in the movie [23_03_2010_1_short.AVI]. Further upstream ($x'/d_o > 4$), the negative wave propagated in a more gradual, gentle manner during which its leading edge was very flat and barely perceptible. The wave celerity decreased slowly with increasing distance from the gate as illustrated in Figure 4.

3.2 Instantaneous free-surface and velocity measurements

During the negative wave, the water depth decreased relatively gradually after the initial surge formation. The free surface measurements showed some surface curvature near the surge leading edge. The longitudinal velocity component increased at the same time as the water depth decreased. Typical results are presented in Figures 5, 6 and 7. Figure 5 presents some free-surface measurements at $x = 6$ and 10.5 m; both the ensemble-median, the difference between maximum and minimum water depths ($d_{max}-d_{min}$) and the difference between the 3rd and 1st quartiles ($d_{75}-d_{25}$) are presented. Figures 6 and 7 show some velocity measurements at $x = 10.5$ m and $x = 6$ m respectively. Each graph includes the ensemble-median water depth, the median velocity components and difference between the 3rd and 1st quartiles ($V_{75}-V_{25}$).

The free-surface data highlighted the gentle free-surface profile at the leading edge of the negative wave (Fig. 5). Some large fluctuations in free-surface elevations were observed briefly behind the negative wave leading edge: e.g., for $t(g/d_o)^{1/2} = 70$ to 75 and 95 to 105 in Figures 5A and 5B respectively. The free-surface curvature and slope were larger close to the gate ($x = 10.5$ m) than further upstream ($x = 6$ m) (Fig. 5). Based upon the maximum free-surface curvature observations at the wave leading edge, the vertical pressure distributions were calculated using a solution of the Boussinesq equation (Montes and Chanson 1998) and summarised in Table 2. Table 2 includes the radius of curvature of free-surface and deviation from hydrostatic pressure where the free-surface curvature is maximum (Table 2, columns 6 & 7). The results implied that the smallest radius of curvature was large: $|(R_s)_{min}| = 7$ m and 49 m at 0.65 and 5.15 m upstream of the gate respectively (i.e. $x = 10.5$ & 6 m). Simply the pressure distributions at the leading edge were quasi-hydrostatic within the approximations of the theoretical model.

The unsteady velocity measurements were performed at four vertical elevations: $z/d_o = 0.027, 0.104, 0.516$ and 0.563. The results highlighted a number of basic features throughout the water column beneath the negative surge. The longitudinal velocity measurements showed an acceleration of the flow during the drawdown of the free-surface (Fig. 6 & 7). This was associated with some increase in all velocity component fluctuations, compared to the steady state and to the final flow conditions (not shown herein). For example, for $t(g/d_o)^{1/2} = 65$ to 75 and 90 to 120 in Figures 6 and 7

respectively. Figures 6 and 7 show the time-variations of the instantaneous velocity components for the same run (Series 2, Table 1) at two different longitudinal locations: i.e., x = 10.5 m close to the gate (Fig. 6) and x = 6 m (Fig. 7). The magnitude of the difference between 3rd and 1st quartiles (V_{75}-V_{25}) was about similar at both locations (x = 6 & 10.5 m) as illustrated in Figures 6 and 7 drawn with the same horizontal and vertical scales.

The transverse velocity component V_y showed quantitatively lesser fluctuations before, during and after surge formation than in the horizontal and vertical directions. Close to the free-surface (e.g. z/d_o = 0.62), the vertical velocity component was negative on average and its magnitude was comparable to the maximum vertical velocity of the free-surface: that is, $(\partial d/\partial z)_{max}/V_o$ = -1.7 and -0.25 at x = 10.5 and 6 m respectively.

Overall the present data indicated that the negative wave flow was an unsteady three-dimensional turbulent process.

5. UNSTEADY TURBULENT SHEAR STRESSES

5.1 Presentation

A series of twenty five instantaneous free-surface and velocity records were repeated, and the data were synchronised. The ensemble average (EA) technique was applied and the turbulent velocity fluctuation v was calculated as:

$$v = V - \overline{V} \tag{4}$$

where V is the instantaneous velocity and $\overline{V}$ is the ensemble median.

In a turbulent flow, the flux of x-momentum in the y-direction induces a shear stress term in the x-direction: i.e., the turbulent stress $\rho v_x v_y$. The turbulent stress tensor is a transport effect resulting from turbulent motion induced by velocity fluctuations with the subsequent increase of momentum exchange and of mixing (Piquet 1999). In the present study, the turbulent shear stresses were calculated based upon an ensemble-median technique (median value of 25 runs) as Chanson and Docherty (2012). Some typical results are presented in Figure 8.

The experimental results showed a number of basic properties. Overall the turbulent stress data indicated that the passage of a negative surge was associated with large turbulent stresses and turbulent stress fluctuations at all vertical elevations. That is, the magnitude of turbulent Reynolds stress components was significantly larger than in the initially steady flow and than in the final flow after the passage of the wave. This was observed with all Reynolds stress components at both x = 6 and 10.5 m. Although the boundary shear stress in an accelerating flow is lower than that in a steady flow for the same velocity and depth (Johnson 1991, He et al. 2011), the present data highlighted large fluctuations of all velocity components as well as large turbulent stress components in the accelerating flow beneath the

negative wave (Fig. 8). The unsteady Reynolds stress components were significantly larger in the initially steady and final flow motions. The results implied that negative surges have some potential to induce some significant turbulent mixing and to scour natural beds.

5.2 Discussion

Some large magnitude and rapid fluctuations of turbulent Reynolds stresses were observed at all vertical elevations. For a non-cohesive sediment material, the Shields diagram gives a critical shear stress for sediment bed load motion about $(\tau_o)_c$ = 0.1 to 0.5 Pa for fine sand particles with sizes between 0.1 and 1 mm (Graf 1971, Julien 1995). Herein the instantaneous turbulent shear stress magnitudes ranged up to more than 5 Pa (i.e. $v^2/V_o^2 > 0.18$). The Reynolds stress levels were an order of magnitude larger than the critical threshold for sediment motion and transport. For the same fine sand particles with sizes between 0.1 and 1 mm, the ratio of shear velocity to particle fall velocity V_*/w_o ranged from 5 down to 0.5 and may be compared with the threshold for onset of sediment suspension: $(V_*/w_o)_c > 0.2$ to 2 (van Rijn 1984, Chanson 1999). The present data implied that the negative surge motion could scour relatively fine sediment particles and advect these in suspension during the drawdown process. This comparison has some limitations however. The validity of the Shields diagram, critical shear stress estimate and suspension threshold is debatable in a rapidly-varied flow such as a negative wave.

6. CONCLUSION

The unsteady turbulence beneath a negative wave was investigated physically in a series of new experiments conducted in a large rectangular channel with high temporal and spatial resolution. Both the unsteady free-surface profile and turbulence characteristics were measured for a negative surge propagating upstream against an initially steady flow. The velocity measurements were based upon acoustic Doppler velocimetry (ADV) sampled at (200 Hz), and the free-surface elevations were recorded using non-intrusive acoustic displacement meters (ADM) and video imagery. For one set of flow conditions, the experiments were repeated 25 times at two longitudinal locations and four vertical elevations, and the results were ensemble-averaged.

The wave leading edge propagated upstream with a speed which was a function of with time and space. Immediately after the gate opening, the surge leading edge accelerated and its speed increased with time for x' < 4d_o. Further upstream, the negative wave propagated in a gentle with a very flat leading edge which was barely perceptible. The velocity data showed that the upstream propagation of the negative wave was associated with an acceleration of the

flow, while some increased turbulence occurred beneath the wave associated with large velocity fluctuations and large Reynolds stress components. The velocity fluctuations and turbulent stresses were significantly larger than in the initially steady flow and in the final flow motion.

The present results suggested that the negative wave remains a challenging topic and that the unsteady turbulence properties are complicated.

7. ACKNOWLEDGMENTS

10. APPENDIX A - SUPPLEMENTARY VIDEO DATA

Detailed experimental measurements were conducted in a negative wave propagating upstream against an initially steady open channel flow. A series of short movies were further taken during the experiments using a digital video camera Panasonic[TM] NV-GS300 (25 fps). The digital appendix includes two movie files (Table 3). The first movie shows the generation of the negative wave resulting from the rapid gate opening and the following rapidly varied flow motion. The second movie shows the upstream wave propagation about x = 6 m (i.e. about 5.15 m upstream of the gate). The leading edge of the surge is barely perceptible. The list of the movies is detailed in Table 3, including the filenames, file format, and a description of each video. In each movie, the initially steady flow direction is from right to left while the negative wave propagates upstream from left to right.

9. REFERENCES

Bradshaw, P. (1971). "An Introduction to Turbulence and its Measurement." *Pergamon Press*, Oxford, UK, The Commonwealth and International Library of Science and technology Engineering and Liberal Studies, Thermodynamics and Fluid Mechanics Division, 218 pages.

Chanson, H. (1999). "The Hydraulics of Open Channel Flow: An Introduction." *Edward Arnold*, London, UK, 512 pages.

REICHSTETTER, M., and CHANSON, H. (2013). "Unsteady Turbulent Properties in Negative Waves in Open Channels." European Journal of Mechanics B/Fluids, Vol. 37, pp. 1-9 & 2 video movies (DOI: 10.1016/j.euromechflu.2012.07.003) (ISSN 0997-7546).

Chanson, H. (2004). "The Hydraulics of Open Channel Flow: An Introduction." *Butterworth-Heinemann*, 2nd edition, Oxford, UK, 630 pages.

Chanson, H., and Docherty, N.J. (2012). "Turbulent Velocity Measurements in Open Channel Bores." *European Journal of Mechanics B/Fluids*, Vol. 32, pp. 52-58 (DOI 10.1016/j.euromechflu.2011.10.001).

Favre, H. (1935). "Etude Théorique et Expérimentale des Ondes de Translation dans les Canaux Découverts." ('Theoretical and Experimental Study of Travelling Surges in Open Channels.') *Dunod*, Paris, France (in French).

Graf, W.H. (1971). "Hydraulics of Sediment Transport". *McGraw-Hill*, New York, USA.

He, S., Ariyaratne, C., and Vardy, A.E. (2011). "Wall shear stress in accelerating turbulent pipe flow." *Jl Fluid Mech.*, Vol. 685, pp. 440-460 (DOI: 10.1017/jfm.2011.328).

Henderson, F.M. (1966). "Open Channel Flow." *MacMillan Company*, New York, USA.

Johnson, T.V. (1991). "The Study of Unsteady Pipe Flow and Non-Uniform Channel Flow by the Use of Laser Doppler Anemometry." *Ph.D. thesis*, Dept of Civil Engineering, The University of Queensland, Brisbane, Australia.

Julien, P.Y. (1995). "Erosion and Sedimentation." *Cambridge University Press*, Cambridge, UK, 280 pages.

Koch, C., and Chanson, H. (2009). "Turbulence Measurements in Positive Surges and Bores." *Journal of Hydraulic Research*, IAHR, Vol. 47, No. 1, pp. 29-40 (DOI: 10.3826/jhr.2009.2954).

Lauber, G. (1997). "Experimente zur Talsperrenbruchwelle im glatten geneigten Rechteckkanal." ('Dam Break Wave Experiments in Rectangular Channels.') *Ph.D. thesis*, VAW-ETH, Zürich, Switzerland (in German). (also *Mitteilungen der Versuchsanstalt fur Wasserbau, Hydrologie und Glaziologie*, ETH-Zurich, Switzerland, No. 152).

Liggett, J.A. (1994). "Fluid Mechanics." *McGraw-Hill*, New York, USA.

Lighthill, J. (1978). "Waves in Fluids." *Cambridge University Press*, Cambridge, UK, 504 pages.

Montes, J.S. (1998). "Hydraulics of Open Channel Flow." *ASCE Press*, New-York, USA, 697 pages.

Montes, J.S., and Chanson, H. (1998). "Characteristics of Undular Hydraulic Jumps. Results and Calculations." *Journal of Hydraulic Engineering*, ASCE, Vol. 124, No. 2, pp. 192-205.

Piquet, J. (1999). "Turbulent Flows. Models and Physics." *Springer*, Berlin, Germany, 761 pages.

Reichstetter, M., and Chanson, H. (2011). "Physical and Numerical Modelling of Negative Surges in Open Channels." *Hydraulic Model Report No. CH84/11*, School of Civil Engineering, The University of Queensland, Brisbane, Australia, 79 pages.

Rijn, L.C. van (1984). "Sediment transport, Part II: Suspended load transport." *Journal of Hydraulic Engineering*, ASCE, Vol. 110, No. 11, pp. 1613–1641.

REICHSTETTER, M., and CHANSON, H. (2013). "Unsteady Turbulent Properties in Negative Waves in Open Channels." European Journal of Mechanics B/Fluids, Vol. 37, pp. 1-9 & 2 video movies (DOI: 10.1016/j.euromechflu.2012.07.003) (ISSN 0997-7546).

Table 1 - Physical investigation of negative surges: experimental flow conditions

Ref.	Q (m^3/s)	h (m)	d_o (m)	U (m/s)	Instrumentation
(1)	(2)	(3)	(4)	(5)	(6)
Series 1	0.020 & 0.030	0.030 to 0.050	0.10 to 0.26	0.25 to 0.91	Video imagery.
Series 2	0.020	0.030	0.24	0.91	Acoustic displacement meters and ADV (z/d_o = 0.027, 0.104, 0.516, 0.563).

Notes: d_o: initial flow depth measured at x = 6 m; h: undershoot gate height before sudden opening; Q: initially steady

discharge; U: celerity of the negative surge measured at x = 6 m; x: longitudinal distance from the channel upstream

end; z: vertical elevation above the bed.

Table 2 - Maximum free-surface curvature at the leading surge of the negative surge

Q (m3/s)	h (m)	x (m)	$(\partial^2 d/\partial t^2)_{max}$ (m/s^2)	$\partial d/\partial t$ (m/s)	$(R_s)_{min}$ (m)	$1 + \dfrac{(\partial P/\partial z)_{max}}{\rho g}$
(1)	(s)	(3)	(4)	(5)	(6)	(7)
0.020	0.030	6.0	-0.017	-0.007	-48.6 [+]	6×10^{-5} [+]
		10.5	-0.143	-0.066	-6.9 [+]	5.3×10^{-4} [+]

Notes: R_s: radius of curvature; [+]: calculations based upon the Boussinesq equation solution of Montes & Chanson

(1998).

Table 3 - Video movies of negative waves propagating upstream in an open channel

Filename	Format	Description
23_03_2010_1_short.AVI	AVI	Negative wave generation by the rapid gate opening and upstream propagation next to the gate - Duration: 13 s. Run 20100323_1, Q= 0.020 m^3/s, d_o = 0.24 m, S_o = 0.
2010-05-05 13.41.43 ns5.a_very_short. AVI	AVI	Negative wave propagating upstream about x = 6 m - Duration: 11 s. Run 20100505, Q= 0.020 m^3/s, d_o = 0.24 m, S_o = 0.

FIGURE CAPTION

Fig. 1 - Definition sketch of a negative wave propagating upstream in an open channel

Fig. 2 - Initial steady flow free-surface profile prior to negative surge and final free-surface profile after gate opening - Flow conditions: $Q = 0.020$ m^3/s, $h = 0.030$ m, steady flow direction from right to left - Comparison between physical data (recorded with acoustic displacement meters) and backwater calculations

Fig. 3 - Instantaneous free-surface profiles during the negative wave generation and propagation - Initial flow conditions: $Q = 0.030$ m^3/s, $h = 0.040$ m, $d_o = 0.26$ m - Negative wave propagation from left to right - The legend indicates the video frame number

(A) Immediately upstream of the gate ($10.48 < x < 11.2$ m)

(B) About $x = 6$ m ($5.8 < x < 6.3$ m)

Fig. 4 - Dimensionless celerity of the negative wave as a function of the longitudinal distance for $Q = 0.020$ m^3/s, $h = 0.030$ m, $d_o = 0.24$ m - Error bars are included

Fig. 5 - Unsteady free-surface measurements beneath a negative surge: time-variations of the median water depth, difference between maximum and minimum water depths ($d_{max}-d_{min}$) and difference between the 3rd and 1st quartiles ($d_{75}-d_{25}$) - Flow conditions: $Q = 0.020$ m^3/s, $h = 0.030$ m

(A) Water depth data recorded at $x = 10.5$ m (close to the gate)

(B) Water depth data recorded at $x = 6$ m

Fig. 6 - Free-surface and velocity data beneath a negative surge at $x = 10.5$ m (0.65 m upstream of gate): ensemble-median water depth d_{median}, median velocity components and difference between the 3rd and 1st quartiles ($V_{75}-V_{25}$) - Flow conditions: $Q = 0.020$ m^3/s, $h = 0.030$ m, $x = 10.5$ m - Data truncated when ADV unit was out of water

(A) Longitudinal velocity component V_x at $z/d_o = 0.615$

(B) Transverse velocity component V_y at $z/d_o = 0.615$

(C) Vertical velocity component V_z at $z/d_o = 0.615$

REICHSTETTER, M., and CHANSON, H. (2013). "Unsteady Turbulent Properties in Negative Waves in Open Channels." European Journal of Mechanics B/Fluids, Vol. 37, pp. 1-9 & 2 video movies (DOI: 10.1016/j.euromechflu.2012.07.003) (ISSN 0997-7546).
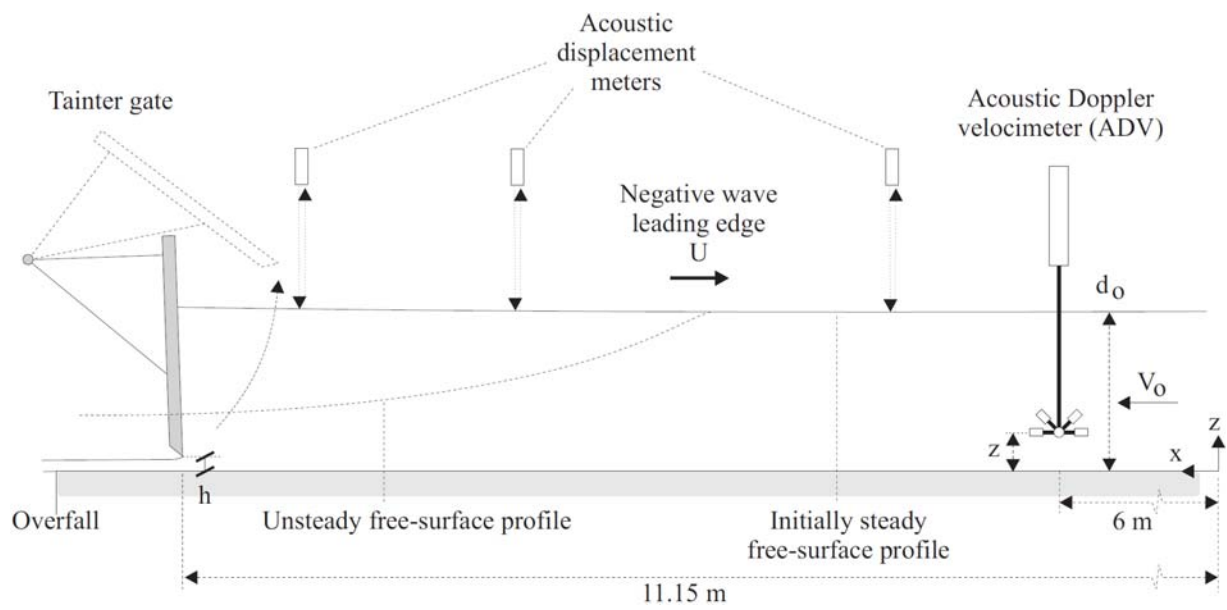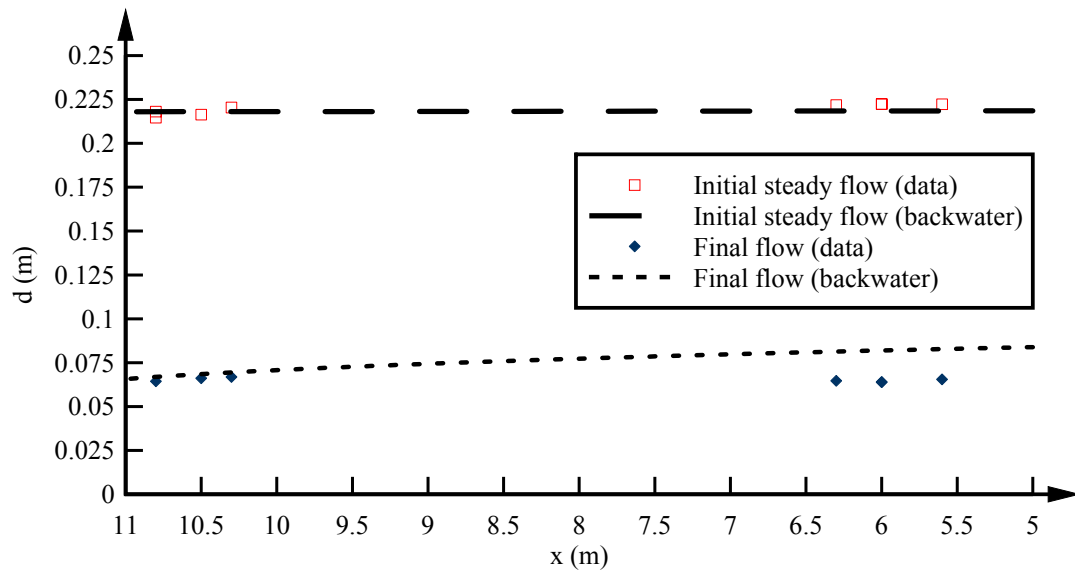
Fig. 7 - Free-surface and velocity data beneath a negative surge at $x = 6$ m (5.15 m upstream of gate): ensemble-median water depth d_{median}, median velocity components and difference between the 3rd and 1st quartiles $(V_{75}-V_{25})$ - Flow conditions: $Q = 0.020$ m^3/s, $h = 0.030$ m, $x = 6.0$ m

(A) Longitudinal velocity component V_x at $z/d_o = 0.563$

(B) Transverse velocity component V_y at $z/d_o = 0.563$

(C) Vertical velocity component V_z at $z/d_o = 0.563$

Fig. 8 - Ensemble-median water depth d_{median} and velocity components, and median turbulent Reynolds stress tensor components beneath a negative surge at $x = 6$ m (5.15 m upstream of gate) and $z/d_o = 0.030$ - Flow conditions: $Q = 0.020$ m^3/s, $h = 0.030$ m, $x = 6.0$ m, $z = 0.0067$ m, $z/d_o = 0.030$

(A) Reynolds stress tensor components ρv_x^2 and $\rho v_x v_y$

(B) Reynolds stress tensor components ρv_y^2 and $\rho v_y v_z$

(C) Reynolds stress tensor components ρv_z^2 and $\rho v_x v_z$

REICHSTETTER, M., and CHANSON, H. (2013). "Unsteady Turbulent Properties in Negative Waves in Open Channels." European Journal of Mechanics B/Fluids, Vol. 37, pp. 1-9 & 2 video movies (DOI: 10.1016/j.euromechflu.2012.07.003) (ISSN 0997-7546).

CAPTION FOR THE SUPPLEMENTARY MATERIAL

23_03_2010_1_short.AVI: Negative wave generation caused by by the rapid gate opening and its upstream propagation in the vicinity of the gate (Duration: 13 s) - Run 20100323_1, Q= 0.020 m3/s, do = 0.24 m, So = 0

2010-05-05 13.41.43 ns5.a_very_short. AVI: Negative wave propagating upstream about x = 6 m (Duration: 11 s) - Run 20100505, Q= 0.020 m3/s, do = 0.24 m, So = 0

Fig. 1 - Definition sketch of a negative wave propagating upstream in an open channel

Fig. 2 - Initial steady flow free-surface profile prior to negative surge and final free-surface profile after gate opening - Flow conditions: Q = 0.020 m^3/s, h = 0.030 m, steady flow direction from right to left - Comparison between physical data (recorded with acoustic displacement meters) and backwater calculations

Fig. 3 - Instantaneous free-surface profiles during the negative wave generation and propagation - Initial flow conditions: Q = 0.030 m³/s, h = 0.040 m, d_o = 0.26 m - Negative wave propagation from left to right - The legend indicates the video frame number

(A) Immediately upstream of the gate (10.48 < x < 11.2 m)

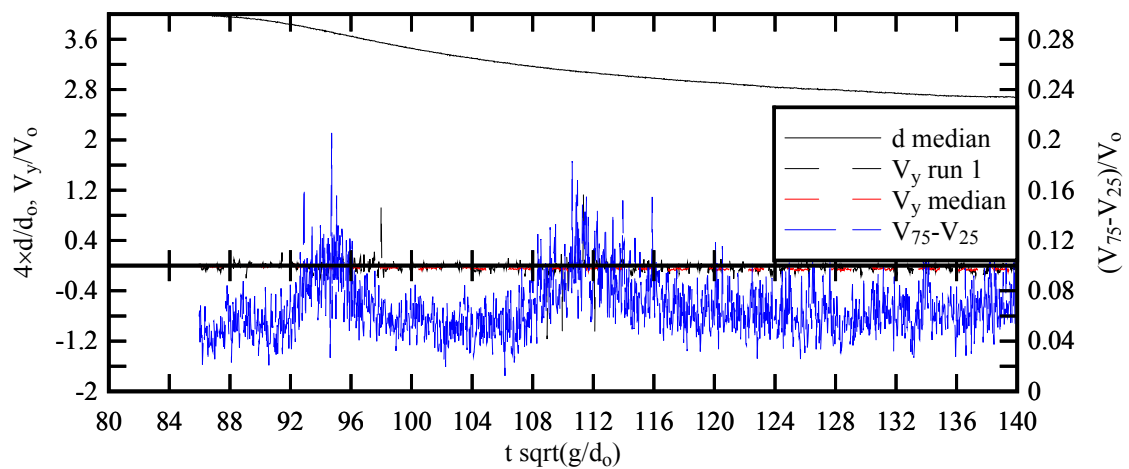

(B) About x = 6 m (5.8 < x < 6.3 m)

REICHSTETTER, M., and CHANSON, H. (2013). "Unsteady Turbulent Properties in Negative Waves in Open Channels." European Journal of Mechanics B/Fluids, Vol. 37, pp. 1-9 & 2 video movies (DOI: 10.1016/j.euromechflu.2012.07.003) (ISSN 0997-7546).

Fig. 4 - Dimensionless celerity of the negative wave as a function of the longitudinal distance for Q = 0.020 m^3/s, h = 0.030 m, d$_o$ = 0.24 m - Error bars are included

Fig. 5 - Unsteady free-surface measurements beneath a negative surge: time-variations of the median water depth, difference between maximum and minimum water depths (d_{max}-d_{min}) and difference between the 3rd and 1st quartiles (d_{75}-d_{25}) - Flow conditions: $Q = 0.020$ m^3/s, $h = 0.030$ m

(A) Water depth data recorded at $x = 10.5$ m (close to the gate)

(B) Water depth data recorded at $x = 6$ m

Fig. 6 - Free-surface and velocity data beneath a negative surge at x = 10.5 m (0.65 m upstream of gate): ensemble-median water depth d_{median}, median velocity components and difference between the 3rd and 1st quartiles (V_{75}-V_{25}) - Flow conditions: Q = 0.020 m³/s, h = 0.030 m, x = 10.5 m - Data truncated when ADV unit was out of water

(A) Longitudinal velocity component V_x at z/d_o = 0.615

(B) Transverse velocity component V_y at z/d_o = 0.615
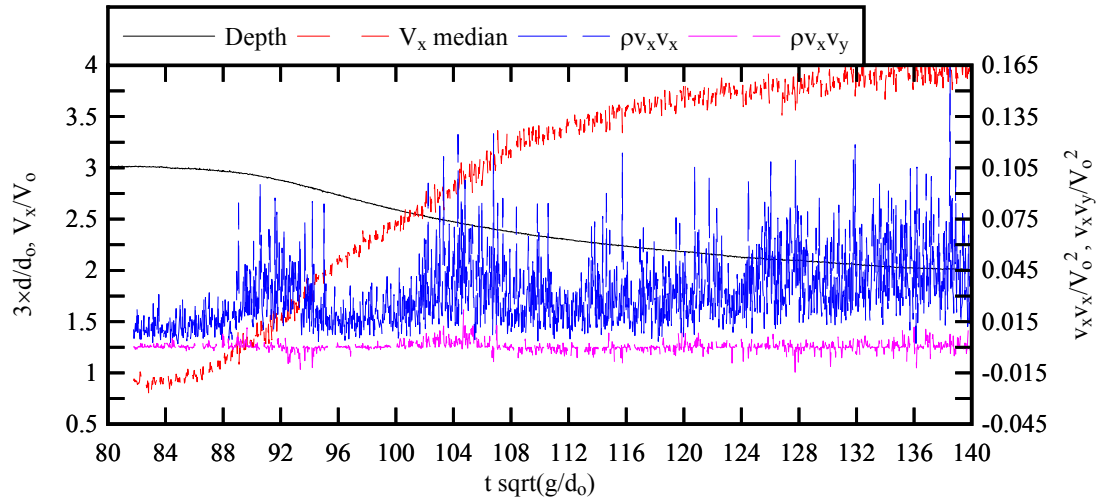

(C) Vertical velocity component V_z at z/d_o = 0.615

Fig. 7 - Free-surface and velocity data beneath a negative surge at x = 6 m (5.15 m upstream of gate): ensemble-median water depth d_{median}, median velocity components and difference between the 3rd and 1st quartiles $(V_{75}-V_{25})$ - Flow conditions: Q = 0.020 m^3/s, h = 0.030 m, x = 6.0 m

(A) Longitudinal velocity component V_x at z/d_o = 0.563

(B) Transverse velocity component V_y at z/d_o = 0.563

(C) Vertical velocity component V_z at z/d_o = 0.563

Fig. 8 - Ensemble-median water depth d_{median} and velocity components, and median turbulent Reynolds stress tensor components beneath a negative surge at x = 6 m (5.15 m upstream of gate) and $z/d_o = 0.030$ - Flow conditions: Q = 0.020 m^3/s, h = 0.030 m, x = 6.0 m, z = 0.0067 m, $z/d_o = 0.030$

(A) Reynolds stress tensor components ρv_x^2 and $\rho v_x v_y$

(B) Reynolds stress tensor components ρv_y^2 and $\rho v_y v_z$

(C) Reynolds stress tensor components ρv_z^2 and $\rho v_x v_z$